Directional solidification near minimum c_∞: Two-dimensional isolas and multiple solutions

G. J. Merchant and S. H. Davis
Department of Engineering Sciences and Applied Mathematics, Northwestern University, Evanston, Illinois 60208
(Received 10 July 1989)

Mullins and Sekerka showed, using linear-stability theory, that for fixed temperature gradient, the planar interface is stable for all pulling speeds V when the solute concentration $c_\infty < c_\infty^*$. When $c_\infty > c_\infty^*$, there is a low-speed instability when the melt is constitutionally undercooled and a high-speed stabilization due to surface energy when the absolute-stability criterion is reached. The two branches meet at c_∞^*. In this paper two-dimensional weakly nonlinear instabilities are studied for small $|c_\infty - c_\infty^*|$ so both the low- and high-speed bifurcations can be simultaneously described. When the thermal-conductivity ratio $n = k_S/k_L$ is small (large), both bifurcations are supercritical (subcritical) and shallow (deep) cells emerge. For intermediate n there is complex behavior exhibiting multiple transitions, separated branches (isolas), and multiple cellular states.

I. INTRODUCTION

When a dilute binary mixture is directional-solidified, the initially planar solidification front undergoes an instability that depends on values of the various control parameters: the concentration c_∞ of solute, the temperature gradient G, and pulling speed V.

Experimentally it has been found[1,2] for fixed G and c_∞ that for low speeds V the planar interface is stable; at some critical speed the planar interface undergoes a transition to cellular structure with well-defined wavelength λ. As V is increased further, the cell roots deepen until there is a dendritic transition. At high enough pulling speeds the effect of surface energy begins to dominate; there is a transition from dendrites to cells whose amplitudes slowly diminish with increasing V until another critical pulling speed is reached at which the planar interface regains stability.

In order to predict these critical values Mullins and Sekerka[3] carried out a linear-stability analysis of the planar front. They examined the effects of perturbations to the interface of the form $\exp(\sigma t + iax)$, where σ is the growth rate and a is the wave number in the x direction along the planar interface. Under neutral conditions, $\sigma = 0$, they found values for the critical pulling speed V_c and wave length λ_c for the onset of instability and values of V_a and λ_a, where the planar interface regains stability. In Fig. 1 we show the neutral stability curve for a SCN-acetone mixture (where SCN is succinonitrile) directionally solidified at a temperature gradient of $G = 150$ K/cm. From this it can be seen that there exist two branches of the neutral stability curve. The lower branch, corresponding to the onset of instability $V = V_c$, is associated with the constitutional undercooling condition which is a balance between solute rejection and thermal stabilization. Below this branch the planar interface is stable. The upper branch, corresponding to $V = V_a$, is called the absolute stability limit and balances solute rejection with surface energy. Above this branch the planar interface is stable. Both stability branches join to form a limit point located at (c_∞^*, V^*). The solid line indicates where the weakly nonlinear theory (to be described below) predicts smooth transitions to shallow two-dimensional cells; the dashed line shows the region where jump transitions in the interface are predicted to occur. The *transition point* that separates these is denoted by TP. Similar neutral curves for the Al-Cu mixture at a temperature gradient of 200 K/cm have appeared in Coriell and Sekerka[4] and Coriell *et al.*[5]

In order to follow the time evolution of the solid/liquid interface, Wollkind and Segel[6] ignored the effects of latent heat and performed a two-dimensional weakly nonlinear analysis valid near the neutral curve. They derived an evolution equation for the leading-order disturbance amplitude A,

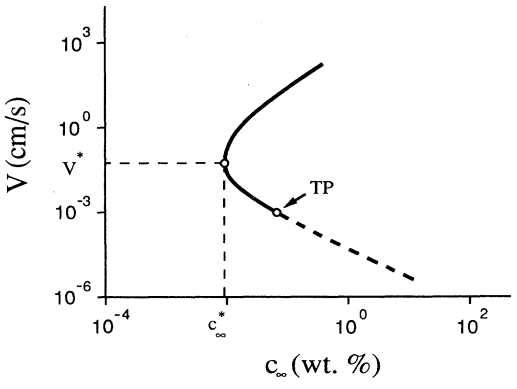

FIG. 1. Neutral stability curve for SCN-acetone at a temperature gradient $G = 150$ K/cm. The region inside the curve corresponds to an unstable planar interface. The dashed lines indicate regions of subcritical bifurcation (Ref. 7), the solid line supercritical bifurcation (Ref. 7), and TP denotes the transition point that separates these. The limit point is located at (c_∞^*, V^*).

$$\frac{dA}{dt}=\sigma A-a_1 A|A|^2 . \tag{1.1}$$

Here σ is the linear theory growth rate, while a_1 is the Landau coefficient. If it turns out that $a_1>0$, then small amplitude steady-state two-dimensional cells exist and the bifurcation is termed supercritical; if $a_1<0$, then no small amplitude steady states exist and as $V\to V_c^-$, the disturbance jumps to some finite-amplitude state through a subcritical bifurcation. The position where $a_1=0$ identifies the transition point.

Alexander *et al.*[7] included the effects of latent heat in the weakly nonlinear analysis of Wollkind and Segel.[6] They found that latent heat is important in the nonlinear theory when the ratio n of thermal conductivities of solid to liquid, respectively, is near unity.

Merchant and Davis[8] presented the two-dimensional bifurcation results of Alexander *et al.*[7] on the neutral stability curve for a SCN-acetone system and showed that the effect of latent heat with n near unity is to extend the region of supercritical bifurcation into experimentally accessible parameter ranges.

In directional solidification standard length and time scales are D/V and D/V^2, respectively, where D is the diffusion coefficient of solute in the liquid phase. If these are used to nondimensionalize the system, the control parameters become the morphological number M, which measures the degree of constitutional undercooling, Γ a measure of surface energy, and k the segregation coefficient measuring the amount of solute rejected (or incorporated) at the interface. Sivashinsky[9] noted that as the segregation coefficient k approached zero, $M\to 1$ with the nondimensional $\lambda_c\to\infty$. By taking advantage of the long-wave behavior for small k, he derived an evolution equation valid for M near 1, and found the bifurcation to two-dimensional cells to be subcritical. Brattkus and Davis[10] identified another long-wave limit near absolute stability and derived a strongly nonlinear evolution equation. Here they found that the bifurcation to cells is supercritical. This was also observed experimentally by Trivedi *et al.*[2] Recently, Riley and Davis[11] were able to extend the small-k analysis to systems with large Γ, and they derived successive evolution equations valid for all values of M and, in the frozen temperature approximation (equal thermal conductivities and negligible latent heat), they found the transition point between subcritical and supercritical behavior to be located at $M=\frac{9}{4}$. These equations are thus intermediate between those of Sivashinsky[9] and Brattkus and Davis.[10]

In most of the previous analytical work the control parameters used were proportional to the morphological number M and the surface energy Γ. Unfortunately, a system controlled using these parameters no longer has the pulling speed V isolated as a control parameter, and the relationship with the underlying experimental situation is often lost. In order to isolate the control parameters that reflect the operation of an experiment, but retain the advantages of nondimensional variables, Ungar and Brown[12] introduced a reference wavelength λ^* and used the Peclet number $P=V\lambda^*/D$ as the control parameter. They numerically follow the bifurcation structure for large amplitude disturbances using periodic boundary conditions. In treating the solidification model as a pure bifurcation problem with V as the bifurcation parameter Haug[13] considered the interaction of discrete wavelengths, allowed by considering solidification in a very small periodic box, and identified the normal forms possible using symmetry arguments but never identified when they occurred. Also his analysis was restricted to k and n near unity.

We choose a different approach and introduce new length and time scales based on the capillary length, in a similar fashion to Haug,[13] and redraw the neutral stability curves in new control parameters proportional to V and c_∞. These curves retain the features of the dimensional version discussed earlier and shown in Fig. 1.

In these control variables there is a limit point of the neutral stability curve, and by analyzing a neighborhood of this limit point we are able to simultaneously capture the interfacial transitions to two-dimensional cells at both $V=V_c$ and $V=V_a$. By performing a weakly nonlinear analysis in this region we derive two new amplitude equations describing the time evolution of the most unstable disturbance. The first, containing cubic nonlinearities, is valid when the transition point is an $O(1)$ distance from the limit point as $c_\infty\to c_\infty^*$. When the transition point is an $O(|c_\infty-c_\infty^*|^{1/4})$ distance away from the limit point, the original amplitude equation derived is no longer valid and a higher-order equation, including both cubic and quintic nonlinearities, applies. These amplitude equations describe a rich variety of transitions to steady two-dimensional cells and are able to show the asymmetry of the bifurcation structure present near both $V=V_c$ and $V=V_a$. Interesting phenomena such as disconnected solution branches are found in regions where linear theory predicts stability. Bifurcation structures which bend back over themselves leading to the possibility of large jump transitions are also found.

II. FORMULATION

The aim is to isolate the control parameters V and c_∞. New length δ_L and time δ_T scales, independent of V and c_∞, are chosen based on capillary scales; these are

$$\delta_L=(\gamma T_M/LG_L)^{1/2} \tag{2.1a}$$

and

$$\delta_T=\gamma T_M/LG_L D , \tag{2.1b}$$

respectively. Here T_M is the melting point of the pure solvent, γ is the interfacial energy, L the latent heat, and G_L the temperature gradient in the liquid at the interface. In the analysis to follow, G_L is taken to be independent of V. This assumption is valid as long as the length $\bar{L}$ (in the z direction) of the experimental box satisfies $\bar{L}\ll\kappa_{(L,S)}/V$, where $\kappa_{(L,S)}$ are thermal diffusion coefficients for the liquid and solid phases. For low speeds this is the case, but for higher speeds (perhaps near absolute stability) this assumption may be violated. In this case curvature in the temperature field is important. For high-enough pulling speeds interface attach-

ment kinetics would also become important.

The solidification system,[6] in a reference frame moving at speed V with the interface, rescaled using (2.1) as length and time scales, becomes

liquid: $z > h(x,t)$,

$$\nabla^2 c + \mathcal{V} c_z = c_t \ , \tag{2.2a}$$

$$\nabla^2 T_L = 0 \ ; \tag{2.2b}$$

solid: $z < h(x,t)$,

$$\nabla^2 T_S = 0 \ ; \tag{2.2c}$$

interface: $z = h(x,t)$,

$$T_L = T_S = \mathcal{C} c + h_{xx}(1+h_x^2)^{-3/2} \ , \tag{2.2d}$$

$$(1+h_t)[1+(k-1)c] = c_z - h_x c_x \ , \tag{2.2e}$$

$$l(1+h_t) = n(T_{S_z} - h_x T_{S_z}) - (T_{L_z} - h_x T_{L_x}) \ , \tag{2.2f}$$

where

$$\mathcal{V}^2 = \frac{\gamma T_M V^2}{L G_L D^2} \ , \tag{2.3a}$$

$$\mathcal{C}^2 = \frac{m^2(k-1)^2 L c_\infty}{k^2 G_L \gamma T_M} \ , \tag{2.3b}$$

and

$$l^2 = \frac{L^2 D^2}{k_L^2 G_L T_m}\left[\frac{L}{\gamma}\right] \tag{2.3c}$$

are pulling speed, concentration of solute, and latent-heat parameters, respectively. The temperature in the solid and liquid phases (T_S, T_L) is scaled on G_L multiplied by δ_L, and the concentration c is scaled on the concentration gradient on the liquid side G_c multiplied by δ_L. Here k_L (k_S) is the thermal conductivity of the liquid (solid) phase and the ratio k_S/k_L is denoted by n. The additional dimensional parameters are the slope m of the liquidus, and the segregation coefficient k. In deriving system (2.2) it is assumed that the specific heats in both phases are equal, c_∞ is small so that the phase diagram is locally linear, convection in the melt is absent, there is negligible solute diffusion in the solid, and the ratio of solute diffusion to thermal diffusion is much less than unity.

A linear-stability analysis of the planar interface is performed by examining perturbations of the form $\exp(\sigma t + iax)$, where the nondimensional wave number a and growth rate σ are now scaled on δ_L and δ_T, respectively. The characteristic equation obtained is

$$\sigma = \frac{a\{\mathcal{V}\mathcal{C}(1+n)(\lambda_1 - \mathcal{V}) - [\lambda_1 + \mathcal{V}(k-1)][2 + l\mathcal{V} + a^2(1+n)]\}}{l[\lambda_1 + \mathcal{V}(k-1)] + (1+n)\mathcal{C}a} \ , \tag{2.4a}$$

where

$$\lambda_1 = \tfrac{1}{2}\{\mathcal{V} + [\mathcal{V}^2 + 4(a^2+\sigma)]^{1/2}\} \ . \tag{2.4b}$$

For $\mathrm{Re}(\sigma) > 0$, the solidification interface is unstable, and for $\mathrm{Re}(\sigma) < 0$, it is stable. The principle of exchange of stabilities holds for this system[7] so that the neutral stability curve is obtained by setting $\sigma = 0$ in (2.4). A neutral curve in the $(\mathcal{C}, \mathcal{V})$ plane for $l = 1.0$, $n = 2.0$, and $k = 0.2$ is shown in Fig. 2. This curve retains all of the features present in the dimensional neutral curve of Fig. 1. The upper branch of the neutral stability curve approaches the absolute stability asymptote $\Gamma = 1/k$, or

$$\mathcal{V} = \mathcal{C}/k \ . \tag{2.5a}$$

The lower branch approaches the constitutional undercooling asymptote $M = 1$, or

$$\mathcal{V} = \frac{2}{\mathcal{C}(1+n) - l} \ . \tag{2.5b}$$

One substantial difference between these new scalings compared to the old is reflected in the wave number a, which is now independent of pulling speed. As $\mathcal{C} \to \infty$, near absolute stability $a_c \to \infty$, while on the lower branch, $a_c \to 0$. A diagram of the neutral stability curve in the $(\mathcal{C}, a)$ plane is given in Fig. 3 with $l = 1.0$, $n = 2.0$, and $k = 0.2$. Taking a cross section of the neutral stability curve in the $(\mathcal{C}, \mathcal{V})$ plane at a fixed value of $\mathcal{C} = 4.0$ gives the variation of critical wave number with $\mathcal{V}$. This is shown in Fig. 4. Near the onset of instability, as noted by Bennett and Brown,[14] the neutral curve is very flat and so wavelength selection is weak. Near absolute stability the presence of latent heat sharpens the neutral curve,[15] thus creating the possibility of well-defined wavelength selection. Of course, this conclusion may be altered by

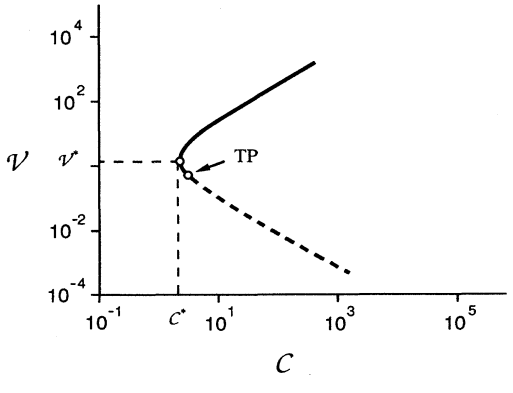

FIG. 2. Neutral stability curve for planar growth in the $(\mathcal{C}, \mathcal{V})$ plane. The region inside the curve corresponds to an unstable planar interface. The dashed lines indicate regions of subcritical bifurcation (Ref. 7), the solid line supercritical bifurcation (Ref. 7), and TP denotes the transition point that separates these. The limit point is located at $(\mathcal{C}^*, \mathcal{V}^*)$.

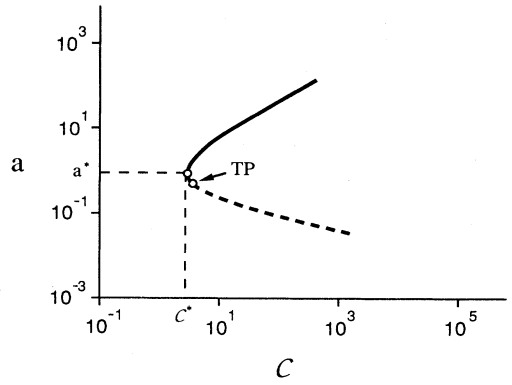

FIG. 3. Neutral stability curve for planar growth in the $(\mathcal{C},a)$ plane. The region inside the curve corresponds to an unstable planar interface. The dashed lines indicate regions of subcritical bifurcation (Ref. 7), the solid line supercritical bifurcation (Ref. 7), and TP denotes the transition point that separates these. The limit point is located at $(\mathcal{C}^*,a^*)$.

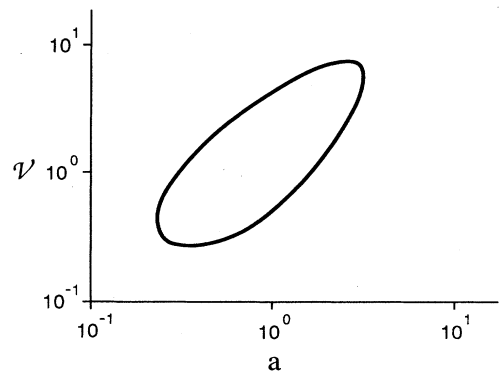

FIG. 4. Neutral stability curve for planar growth in the $(a,\mathcal{V})$ plane. This is a cross section of Fig. 2 taken at $\mathcal{C}=4.0$. Due to the effects of latent heat the curve is much sharper near absolute stability than at the onset of instability.

other effects that are important at high pulling speeds and not included in the current solidification model such as attachment kinetics. The wave number of the most unstable disturbance changes considerably depending on whether the system is operating near the onset of instability, $\mathcal{V}=\mathcal{V}_c$ or near absolute stability, $\mathcal{V}=\mathcal{V}_a$.

An interesting feature of Fig. 2 is the occurrence of a limit point in $\mathcal{C}$. For all $\mathcal{C}$ above a critical value $\mathcal{C}^*$ the planar interface is linearly unstable for all pulling speeds $\mathcal{V}$ in the range $\mathcal{V}_c<\mathcal{V}<\mathcal{V}_a$. As $\mathcal{C}$ approaches $\mathcal{C}^*$ both $\mathcal{V}_c$ and $\mathcal{V}_a$ coalesce; when $\mathcal{C}<\mathcal{C}^*$, the interface is linearly stable for all pulling speeds. This was also noted by Kelly and Ungar.[15] The solidification model used is valid for small concentrations of solute and at moderate pulling speeds. Near the limit point of Fig. 2, $\mathcal{C}$ is certainly small, while $\mathcal{V}$ is moderate (except in the small k limit as will be shown in the next section) suggesting that the Mullins and Sekerka[3] model considered is valid in this region. The coordinates of this limit point, in the absence of latent heat ($l=0$), are easily found to be

$$a^*=\left[\frac{2}{n+1}\right]^{1/2}, \tag{2.6a}$$

$$\mathcal{C}^*=\left[\frac{2}{n+1}\right]^{1/2}\frac{q^{3/2}}{(q-2k)}, \tag{2.6b}$$

$$\mathcal{V}^*=\left[\frac{2}{n+1}\right]^{1/2}\frac{2}{q^{1/2}}, \tag{2.6c}$$

where

$$q=\tfrac{1}{2}[4k-1+(1+8k)^{1/2}]. \tag{2.6d}$$

In this new scaling, the critical wave number near the limit point is $O(1)$. If latent heat is included $\mathcal{V}^*$ is found by solving

$$lk(n+1)^2(k-1)\mathcal{V}^5+k(n+1)[2(k-1)(n+1)-kl^2]\mathcal{V}^4-8kl(n+1)\mathcal{V}^3+4(n+1)(1-4k)\mathcal{V}^2+32=0, \tag{2.7}$$

with $\mathcal{C}^*$ given by

$$\mathcal{C}^*=\frac{(4+l\mathcal{V}^*)[8+kl\mathcal{V}^{*3}(n+1)(k-1)]}{(n+1)\mathcal{V}^*[8-k(n+1)\mathcal{V}^{*2}(2+l\mathcal{V}^*)]}. \tag{2.8}$$

As mentioned in Merchant and Davis[8] the location of the transition point varies depending on the choice of l, n, and k and is especially sensitive to changes in l when n is near unity. In certain parameter ranges the transition point can be made to lie on, or a little above or below the limit point; this feature is important when considering a bifurcation analysis near this limit point.

If we define a small parameter ϵ^2 as the difference between $\mathcal{C}$ and $\mathcal{C}^*$, namely,

$$\mathcal{C}=\mathcal{C}^*+\epsilon^2, \tag{2.9a}$$

then near the limit point the appropriate scalings hold

$$\mathcal{V}=\mathcal{V}^*+\epsilon\bar{\mathcal{V}}, \tag{2.9b}$$

$$a=a^*+\epsilon\bar{a}, \tag{2.9c}$$

$$\sigma=\epsilon^2\bar{\sigma}, \tag{2.9d}$$

where all barred quantities are of unit order as $\epsilon\to 0$. These scaled variables lead to an approximate characteristic equation, valid near the limit point, of the form

$$\bar{\sigma}+\alpha_4\bar{a}^2+\alpha_3\bar{a}\bar{\mathcal{V}}+\alpha_2\bar{\mathcal{V}}^2=\alpha_1, \tag{2.10}$$

where the $\alpha_i(n,k)$ are constants that are given in Appendix B. The approximate characteristic equation is a rotated ellipse in the $(\bar{a},\bar{\mathcal{V}})$ plane. This was observed nu-

merically in Brown[16] for c_∞ near c^*_∞.

In the next section we relate these new control parameters $\mathcal{C}$, $\mathcal{V}$, and l with the most commonly used nondimensional parameters. To clarify our different approach we present some familiar small k results.

III. COMPARISONS WITH PREVIOUS WORK

A. Conversions

When lengths and time are scaled on the solute diffusion scales, $D/V, D/V^2$, respectively, the resulting nondimensional parameters are the morphological number

$$M=\frac{mG_c}{G^*}=\frac{m(k-1)c_\infty V(k_L+k_S)}{kD(k_L G_L+k_S G_S)}\ , \tag{3.1a}$$

where G^* is an average temperature gradient and G_S is the temperature gradient in the solid at the interface. There is a surface energy parameter

$$\Gamma=\frac{\gamma T_M k}{Lm(k-1)c_\infty}\frac{V}{D}\ , \tag{3.1b}$$

and a Stefan number

$$L_H=\frac{LV}{k_L G_L}\ . \tag{3.1c}$$

In this scaling M, Γ, and the segregation coefficient k are taken to be the control parameters. Another commonly used notation (cf. Coriell *et al.*[5]) is then related by

$$G=\frac{1}{M}\ , \tag{3.2a}$$

$$A=k\Gamma\ , \tag{3.2b}$$

and

$$I=\frac{(2+L_H)M}{L_H}\ . \tag{3.2c}$$

These are also similar to those used by Caroli *et al.*[17] and Alexander *et al.*[7]

The morphological number, surface energy parameter and Stefan number are related to $\mathcal{V}$, $\mathcal{C}$, and l by

$$M=\frac{\mathcal{V}\mathcal{C}(1+n)}{2+l\mathcal{V}}\ , \tag{3.3a}$$

$$\Gamma=\mathcal{V}/\mathcal{C}\ , \tag{3.3b}$$

$$L_H=\mathcal{V}l\ . \tag{3.3c}$$

B. Small k

The limit of small segregation coefficient is both physically relevant and mathematically attractive. It is well known for $k\ll 1$, $M_c\to 1$, and, in the old scalings, that the system loses stability to long-wave disturbances. This long-wavelength property has been used by Sivashinsky,[9] Brattkus and Davis,[10] and Riley and Davis.[11] To relate these results to our new scalings we first consider the frozen temperature model $n=1$, $l=0$.

The neutral stability curve always lies between the two stability asymptotes, namely, absolute stability (2.5a) and constitutional undercooling (2.5b). These asymptotes intersect at

$$\mathcal{V}=k^{-1/2},\quad \mathcal{C}=k^{1/2}\ . \tag{3.4}$$

For small k the coordinates of the limit point (2.6), with $n=1$, reduce to

$$\mathcal{V}^*\sim k^{-1/2},\quad \mathcal{C}^*\sim 4k^{1/2}\ , \tag{3.5}$$

indicating that the limit point approaches the intersection of the two stability asymptotes, while both simultaneously move off to infinity. In the frozen temperature approximation $M=\mathcal{V}\mathcal{C}$ so for small k, the limit point is located at $M=4$, and the transition point at $M=\frac{9}{4}$. This is shown in Fig. 5 using $k=0.001$. Thus $M=1$ is always in a region of subcritical bifurcation, in agreement with Sivashinsky.[9]

Another interesting observation is in the small-k limit the approximate characteristic Eq. (2.10) reduces to

$$\bar{\sigma}+(2+\cdots)\bar{a}^2+(k+\cdots)\bar{\mathcal{V}}^2-(2k^{1/2}+\cdots)\bar{a}\bar{\mathcal{V}}=\left[\frac{2}{n+1}\right]^{1/2}(k^{-1/2}+\cdots)\ . \tag{3.6}$$

In order to retain the elliptical nature of (3.6), $\bar{\mathcal{V}}$ and $\bar{a}$ must be rescaled with $\bar{a}/\bar{\mathcal{V}}=k^{1/2}\ll 1$, implying that for small k the neutral curve gets thin and sharp near both the onset of instability and at absolute stability, thus enhancing wavelength selection. Also there is a smaller disparity between the critical wavelengths corresponding to $\mathcal{V}_c$ and $\mathcal{V}_a$.

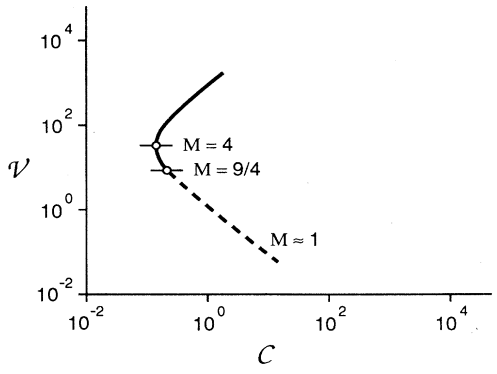

FIG. 5. Neutral stability curve for planar growth in the $(\mathcal{C},\mathcal{V})$ plane, using the frozen temperature approximation, for small k, $k=0.001$. The region inside the curve corresponds to an unstable planar interface. The dashed lines indicate regions of subcritical bifurcation (Ref. 7), the solid line supercritical bifurcation (Ref. 7). The limit point is located at $M=4$ and the transition point at $M=\frac{9}{4}$. The region given by $M\approx 1$ is located in a area of subcritical bifurcation as predicted by Sivashinsky (Ref. 9).

IV. WEAKLY NONLINEAR ANALYSIS

We are interested in the nonlinear behavior near the limit point. We derive an amplitude equation describing the time evolution of the leading-order disturbance amplitude, that captures simultaneously transition to cells near both the lower branch at $\mathcal{V}=\mathcal{V}_c$ and near the upper branch at $\mathcal{V}=\mathcal{V}_a$. Two distinct limits will be considered. When the transition point is away from the limit point, we obtain either supercritical or subcritical bifurcation from both branches via an amplitude equation with cubic nonlinearity. When the transition point approaches the limit point, the amplitude equation has both cubic and quintic nonlinearities and is capable of describing more elaborate modes of transitions to cells.

A. Transition point distant from limit point

At the limit point, where both critical pulling speeds coalesce as $\mathcal{C}\to\mathcal{C}^*$, we expect an isola (a closed curve of solution branches) to form with its center located at $(\mathcal{C}^*,\mathcal{V}^*)$. The structure of this isola is then captured by a perturbation expansion about its center in a small parameter ϵ that is proportional to $(\mathcal{C}-\mathcal{C}^*)^\alpha$, with α appropriately determined (see Dellwo *et al.*[18]).

We consider the solidification model with zero latent heat, though the thermal conductivities in the solid and liquid are allowed to be distinct. The analysis is slightly simplified by this choice but latent heat could be included.

A small parameter ϵ is defined by

$$\mathcal{C}=\mathcal{C}^*+s\epsilon^2 \quad (\alpha=\tfrac{1}{2}) , \tag{4.1}$$

where $s=\pm1$ depending on whether $\mathcal{C}$ is above or below the limit point. A scaled bifurcation parameter is introduced

$$\mathcal{V}=\mathcal{V}^*+\epsilon\mathcal{V}_1+\epsilon^2\mathcal{V}_2+\cdots , \tag{4.2}$$

along with a slow evolution time scale

$$\tau=\epsilon^2 t . \tag{4.3}$$

The preceding scalings are suggested from the linear theory. The governing system is given by (2.2) with $l=0$, and the time derivatives replaced by $\epsilon^2\partial/\partial\tau$. A solution is sought in the form

$$c=\bar{c}(z)+\epsilon c_1(x,z,\tau)+\epsilon^2 c_2(x,z,\tau)+\cdots , \tag{4.4a}$$

$$T_{S,L}=\bar{T}_{S,L}(z)+\epsilon T_{S,L_1}(x,z,\tau)+\epsilon^2 T_{S,L_2}(x,z,\tau)+\cdots , \tag{4.4b}$$

$$h=\bar{h}+\epsilon h_1(x,\tau)+\epsilon^2 h_2(x,\tau)+\cdots , \tag{4.4c}$$

where the barred quantities denote the basic state given by

$$\bar{c}(z)=1-e^{-\mathcal{V}z} , \tag{4.5a}$$

$$\bar{T}_L=z , \tag{4.5b}$$

$$\bar{T}_S=\frac{z}{n} , \tag{4.5c}$$

$$\bar{h}=0 . \tag{4.5d}$$

Note that $\bar{c}$ depends on the bifurcation parameter $\mathcal{V}$. At each order in ϵ there is an eigenvalue problem of the form

$$\left.\begin{aligned}\mathcal{L}\mathbf{c}_i&=\mathbf{r}_i\\ \mathcal{B}\mathbf{c}_i(0)&=\mathbf{d}_i\end{aligned}\right\} \quad i=1,2,\ldots , \tag{4.6}$$

where $\mathbf{c}_i$ is the vector $(c_i,T_{L_i},T_{S_i},h_i)$, $\mathbf{c}_i(0)$ denotes evaluation at $z=0$, and $\mathcal{L}$ and $\mathcal{B}$ are operators from linear theory. These are given by

$$\mathcal{L}\mathbf{c}_i=\begin{bmatrix}\nabla^2 c_i+\mathcal{V}^* c_{i_z}\\ \nabla^2 T_{L_i}\\ \nabla^2 T_{S_i}\\ c_{i_z}(0)+\mathcal{V}^*(1-k)c_i(0)-k\mathcal{V}^{*2}h_i\end{bmatrix} , \tag{4.7a}$$

$$\mathcal{B}\mathbf{c}_i=\begin{bmatrix}T_{L_{i_z}}(0)-nT_{S_{i_z}}(0)\\ h_{i_{xx}}-(1-\mathcal{C}^*\mathcal{V}^*)h_i+\mathcal{C}^* c_i(0)-T_{L_i}(0)\\ h_i\left[1-\frac{1}{n}\right]+T_{L_i}(0)-T_{S_i}(0)\end{bmatrix} . \tag{4.7b}$$

The inhomogeneous terms $\mathbf{r}_i$ and $\mathbf{d}_i$ appear at each order with $\mathbf{r}_1\equiv\mathbf{d}_1\equiv\mathbf{0}$ so that $\mathbf{c}_1$ satisfies the homogeneous linear problem. The solution for $\mathbf{c}_1$ is

$$c_1=-\frac{k\mathcal{V}^{*3}}{2a^{*2}}e^{-\lambda_1 z}A(\tau)e^{ia^*x}+\text{c.c.} , \tag{4.8a}$$

$$T_{L_1}=\frac{1-n}{1+n}e^{-a^*z}A(\tau)e^{ia^*x}+\text{c.c.} , \tag{4.8b}$$

$$T_{S_1}=\frac{n-1}{n(n+1)}e^{a^*z}A(\tau)e^{ia^*x}+\text{c.c.} , \tag{4.8c}$$

$$h_1=A(\tau)e^{ia^*x}+\text{c.c.} , \tag{4.8d}$$

where $A(\tau)$ is a complex amplitude yet to be determined. At each subsequent order a compatability condition must be satisfied by the inhomogeneous terms; this condition is

$$\langle\boldsymbol{\phi},\mathbf{r}_i\rangle+\frac{a^*}{2\pi}\int_0^{2\pi/a^*}\{\bar{d}_{1_i}\phi_2(0)+\bar{d}_{2_i}[\phi_{2_z}(0)-\phi_{3_z}(0)]-\bar{d}_{3_i}\phi_{3_z}(0)\}dx=0 , \tag{4.9}$$

where $\boldsymbol{\phi}$ is the solution of the homogeneous adjoint problem

$$\tilde{\mathcal{L}}\boldsymbol{\phi}=\begin{bmatrix} \nabla^2\phi_1-\mathcal{V}^*\phi_{1_z} \\ \nabla^2\phi_2 \\ \nabla^2\phi_3 \\ \phi_{2_{zxxx}}(0)-\phi_{3_{zxx}}(0)-\left[\frac{1}{n}-\mathcal{C}^*\mathcal{V}^*\right][\phi_{2_z}(0)-\phi_{3_z}(0)]-k\mathcal{V}^{*2}\phi_4-\left[1-\frac{1}{n}\right]\phi_{2_z}(0) \end{bmatrix}=0\ , \tag{4.10}$$

$$\tilde{\mathcal{B}}\boldsymbol{\phi}=\begin{bmatrix} \phi_1(0)-\phi_4 \\ \phi_3(0)-n\phi_2(0) \\ \phi_{3_z}(0)-k\mathcal{V}^*\phi_1(0)+\mathcal{C}^*[\phi_{2_z}(0)-\phi_{3_z}(0)] \end{bmatrix}=0\ . \tag{4.11}$$

The inner product $\langle\ ,\ \rangle$ is given by

$$\langle \mathbf{u},\mathbf{v}\rangle=\frac{a^*}{2\pi}\int_0^{\infty}\int_0^{2\pi/a^*}(u_1\bar{v}_1+u_2\bar{v}_2)dx\,dz+\frac{a^*}{2\pi}\int_{-\infty}^{0}\int_0^{2\pi/a^*}u_3\bar{v}_3dx\,dz+\frac{a^*}{2\pi}\int_0^{2\pi/a^*}u_4\bar{v}_4dx=0\ , \tag{4.12}$$

where the overbar now denotes complex conjugate. At third order in ϵ a restriction is placed on the complex amplitude $A(\tau)$, namely,

$$\frac{dA}{d\tau}=(\alpha_1 s-\alpha_2\mathcal{V}_1^2)A-a_1A|A|^2\ , \tag{4.13}$$

where the α_1, $\alpha_2>0$ are constants determined from linear theory (2.10) and a_1 is the Landau coefficient, which is a function of both n and k. The form of a_1 is

$$a_1=\frac{4}{(n+1)^2}\left[\frac{(1-n)}{(1+n)}F_1(k)+F_2(k)\right]\ , \tag{4.14}$$

where $F_1, F_2>0$ are given in Appendix C.

B. Transition point is coalescent with limit point

Equation (4.13) describes the bifurcation behavior near the limit point when the transition point is distant. Thus $a_1=O(1)$. However a_1 does vary with n and k and can be made to coincide with the limit point. This occurs when $a_1=0$ or

$$n=n_0\equiv\frac{F_1(k)+F_2(k)}{F_1(k)-F_2(k)}\ . \tag{4.15}$$

When n is near n_0 the amplitude equation (4.13) is no longer uniformly valid and the analysis must be generalized with rescaled variables. If the small parameter ϵ is now defined by

$$\mathcal{C}=\mathcal{C}^*+s\epsilon^4\quad(\alpha=\tfrac{1}{4})\ , \tag{4.16}$$

then the rescaled bifurcation parameter is given by

$$\mathcal{V}=\mathcal{V}^*+\epsilon^2\mathcal{V}_2+\epsilon^3\mathcal{V}_3+\cdots\ , \tag{4.17}$$

and n must be near n_0,

$$n=n_0+\epsilon^2 n_2+\cdots\ . \tag{4.18}$$

The sign of n_2 determines whether the transition point lies above or below the limit point. A new slow time scale is also introduced

$$\tau=\epsilon^4 t\ . \tag{4.19}$$

The steps of the preceding analysis are repeated using these new scalings, and at fifth order in ϵ a restriction on $A(\tau)$ is obtained. The new amplitude equation becomes

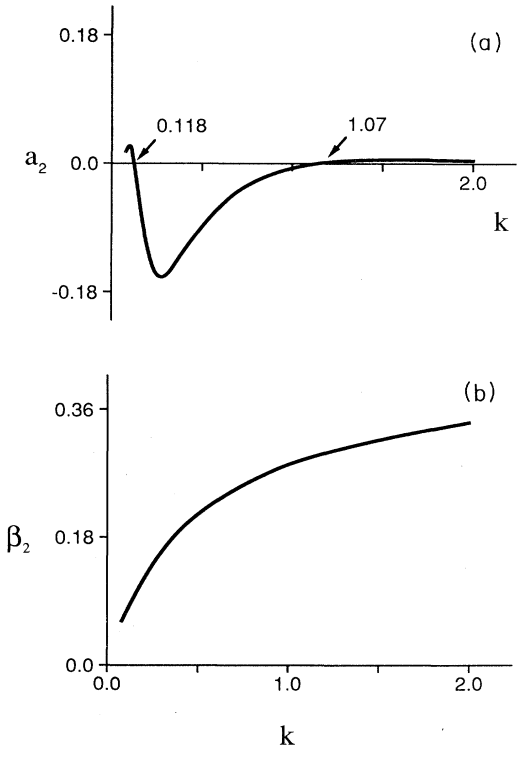

FIG. 6. (a) Graph of the second Landau coefficient a_2 appearing in Eq. (4.20) vs the segregation coefficient k. The two points marked correspond to the zeros of a_2. (b) Graph of the coefficient β_2 appearing in Eq. (4.20) vs the segregation coefficient k.

TABLE I. Please set table caption here.

Region	Coefficients a_2	Δn	p
III	−	+	
IV	−	−	
V	+	+	+
VI	+	−	+
VII	+	+	−
VIII	+	−	−

$$\frac{dA}{d\tau}=(\alpha_1 s-\alpha_2\mathcal{V}_2^2)A -(\beta_1 n_2+\beta_2\mathcal{V}_2)A|A|^2-a_2 A|A|^4 , \quad (4.20)$$

where $a_2(k)$ is a second Landau coefficient, and $\beta_1(k)$, $\beta_2(k)>0$ are two new constants. The constant $\beta_1(k)$ is found to be

$$\beta_1(k)=\frac{8F_1(k)}{(1+n_0)^4} , \quad (4.21)$$

but a_2 and β_2 satisfy extremely long and complicated expressions which were obtained by using a symbolic manipulation program. Due to their complexity, they are not given in this paper but are given in graphical form in Fig. 6. Their signs are given in Table I. This new amplitude equation is valid when the transition point is within order ϵ^2 of the limit point.

C. Recasting

It is easier to grasp the physics contained in the amplitude equations if we return to the original physical variables. If $\hat{A}=\epsilon A$ is the unscaled amplitude of the disturbance and

$$\mathcal{C}\equiv\mathcal{C}^*+\Delta\mathcal{C} , \quad (4.22a)$$

$$\mathcal{V}\equiv\mathcal{V}^*+\Delta\mathcal{V} , \quad (4.22b)$$

so that $\Delta\mathcal{C}$ is the measured distance to the left of the limit point and $\Delta\mathcal{V}$ the corresponding critical pulling speed above the limit point, then (4.13) reduces to

$$\frac{d\hat{A}}{dt}=[\alpha_1\Delta\mathcal{C}-\alpha_2(\Delta\mathcal{V})^2]\hat{A}-a_1\hat{A}|\hat{A}|^2 . \quad (4.23)$$

When n is near n_0, i.e.,

$$n=n_0+\Delta n , \quad (4.24)$$

the amplitude equation (4.20) reduces to

$$\frac{d\hat{A}}{dt}=[\alpha_1\Delta\mathcal{C}-\alpha_2(\Delta\mathcal{V})^2]\hat{A} -(\beta_1\Delta n+\beta_2\Delta\mathcal{V})\hat{A}|\hat{A}|^2-a_2\hat{A}|\hat{A}|^4 . \quad (4.25)$$

The two amplitude equations derived give all possible local transitions from planar to two-dimensional cellular states near the limit point of the neutral curve. For the solidification model considered, the transitions form a two-parameter family of solutions depending on the ratio of thermal conductivities n and the segregation coefficient k. These solutions are discussed in the next section.

V. RESULTS

In Fig. 7 we classify the types of transition from planar to two-dimensional cellular morphology depending on n and k. The lighter interior curve, flanked by two heavier curves, corresponds to the zero of the Landau coefficient a_1 of the amplitude equation (4.23), and is given by Eq. (4.15). Below this curve $a_1>0$, while above, $a_1<0$. There is a singularity in (4.15) when $F_1(k)=F_2(k)$, this corresponds to $k=k^\dagger\approx\frac{1}{16}$. Thus, for small k the transition point never coincides with the limit point of the neutral stability curve; this is in agreement with the small k results of Sec. III. In a band width proportional to $\Delta\mathcal{C}$ about this curve, the transition point is near the limit point and the amplitude equation (4.23) is no longer valid; here (4.25) comes into play.

For the solidification model considered region I is the normal one since n is typically less that 3.0. Here the transition point is below the limit point of the neutral stability curve. In region I, $a_1>0$, and the bifurcation structure is shown as a sequence of three snapshots in Fig. 8(a). The first corresponds to a negative value of $\Delta\mathcal{C}$, so we are looking to the left of the limit point and the planar interface is locally stable for all pulling speeds. In the next frame $\Delta\mathcal{C}=0$, here $\mathcal{V}=\mathcal{V}_c=\mathcal{V}_a$ and the bifurcation structure is just a point. When $\Delta\mathcal{C}>0$, $\mathcal{V}_c$ and $\mathcal{V}_a$ split and the planar interface becomes unstable on the lower branch at a critical pulling speed of

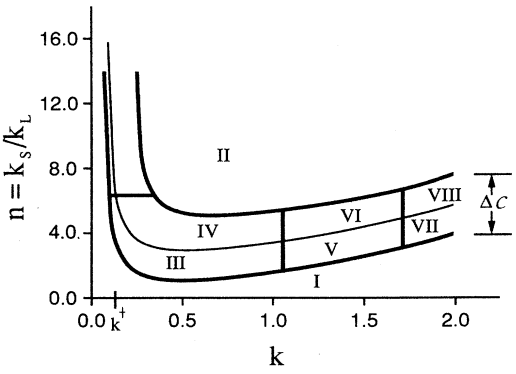

FIG. 7. Regions for which the coefficients of the amplitude Eqs. (4.23) and (4.25) change sign depending on the ratio of thermal conductivities n and the segregation coefficient k. The light curve indicates the position where the Landau coefficient a_1 appearing in Eq. (4.23) vanishes, and is given by Eq. (4.15); it asymptotes to infinity at $k=k^\dagger\approx\frac{1}{16}$. The band of width $O(\Delta\mathcal{C})$ around the light curve denotes the region in which the fifth-order amplitude equation (4.35) is valid. The sign changes occurring in the second Landau coefficient a_2 [as shown in Fig. 6(a)] are given by the two leftmost straight lines, while the vertical line on the right gives the location where p [Eq. (5.1)] changes sign. These sign changes are also summarized in Table I.

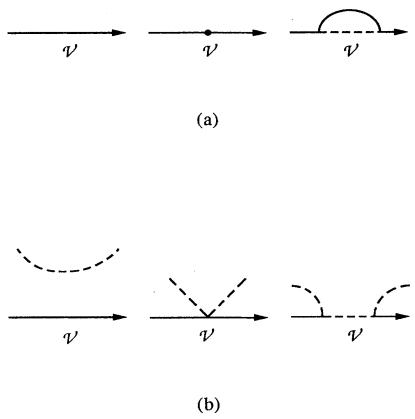

FIG. 8. Bifurcation diagram corresponding to amplitude equation (4.23). The dashed lines represent unstable solutions. (a) region I of Fig. 7; (b) region II of Fig. 7.

$$\mathcal{V}=\mathcal{V}^*-(\alpha_1\Delta\mathcal{C}/\alpha_2)^{1/2}$$

and small amplitude cells begin to develop; the bifurcation is supercritical. These cells increase in amplitude up to a maximum amplitude then begin to fade away with increasing $\mathcal{V}$ until

$$\mathcal{V}=\mathcal{V}^*+(\alpha_1\Delta\mathcal{C}/\alpha_2)^{1/2}\ ,$$

where the planar interface regains stability; again the bifurcation is supercritical. Such behavior has been seen numerically by Kelly and Ungar[15] on the full time-dependent system with latent heat and curvature in the temperature profile. Unlike our work their spatial domain (x direction) is restricted in width to that of a few cell wavelengths by the inclusion of symmetry conditions on either side of the domain. Recently, Trivedi *et al.*[2] performed experiments on a nearly pure sample of carbon tetrabromide and noticed that the bifurcation near $\mathcal{V}_a$ was supercritical and suggested that the bifurcation near $\mathcal{V}_c$ was as well. They also noticed a secondary bifurcation to dendritic solutions at larger amplitudes. Unfortunately they could not measure the amounts or types of impurities present making it difficult to determine c_∞ for comparison with our results. Due to the purity of the sample one might suppose that they were operating relatively near the limit point of the neutral stability curve.

Region II is characterized by quite large conductivity ratios. However, it does exhibit some interesting bifurcation structure. Here $a_1<0$ and the bifurcation structures are shown in Fig. 8(b). The sequence of snapshots is taken at equivalent values of $\Delta\mathcal{C}$ as in Fig. 8(a). To the left of the limit point there exists a disconnected solution branch. Although at this $\mathcal{C}$ the planar interface is linearly stable for all pulling speeds, large enough disturbances will cause the interface to jump to some finite-amplitude cellular state (outside the range of validity of the present theory). For smaller values of $\Delta\mathcal{C}$ this isolated solution branch moves off to infinity. As $\Delta\mathcal{C}$ is increased, this branch moves down towards the axis until $\Delta\mathcal{C}=0$ when it meets the axis at a single point $\mathcal{V}=\mathcal{V}_c=\mathcal{V}_a$. For positive values of $\Delta\mathcal{C}$ the two critical pulling speeds are split, and the planar interface becomes unstable via a jump transition at a pulling speed somewhat below

$$\mathcal{V}=\mathcal{V}^*-(\alpha_1\Delta\mathcal{C}/\alpha_2)^{1/2}\ .$$

At this order in amplitude equation we are unable to close the solution branch, and as $\mathcal{V}$ is increased the interface may go through other transitions until finally when $\mathcal{V}$ is above

$$\mathcal{V}^*+(\alpha_1\Delta\mathcal{C}/\alpha_2)^{1/2}$$

the planar interface regains stability via another jump transition. In region II the transition point is above the limit point and this is reflected by the subcritical nature of both bifurcations.

When the transition point coalesces with the limit point of the neutral curve, the bifurcation structure is described by Figs. 9–11. Table I gives the signs of the coefficients appearing in the amplitude equation (4.25) corresponding to each region. The bifurcation diagrams were drawn using the normal-form characterizations of Golubitsky and Langford.[19]

Figure 9(a) gives the bifurcation structure present in region III. From Table I Δn is positive, indicating that the transition point is located on the lower branch of the neutral stability curve. When operating to the left of the neutral curve there exists a disconnected branch of solutions which moves down from infinity as $\Delta\mathcal{C}$ approaches zero. When $\Delta\mathcal{C}=0$, the two critical pulling speeds are equal and the planar interface is unstable at the single point $\mathcal{V}=\mathcal{V}_c=\mathcal{V}_a$. For a small positive value of $\Delta\mathcal{C}$, $\mathcal{V}_c$ and $\mathcal{V}_a$ split to form a connected supercritical branch on the axis and the disconnected solution branch approaches this. For a larger value of $\Delta\mathcal{C}$, but still to the left of the

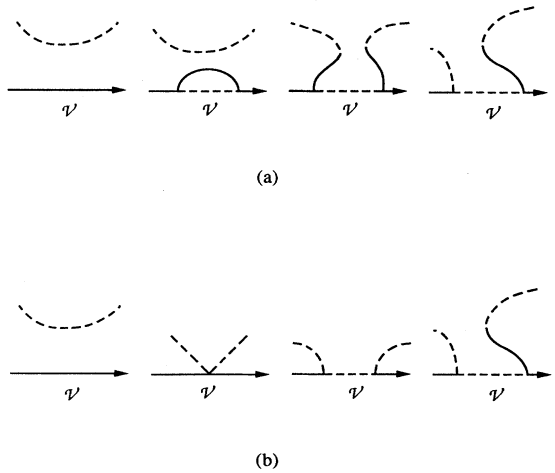

FIG. 9. Bifurcation diagram corresponding to amplitude equation (4.25). The dashed lines represent unstable solutions. (a) region III of Fig. 7; (b) region IV of Fig. 7.

transition point, the disconnected solution attaches to and then opens up the connected solution. Thus, even though the bifurcation to cells is now supercritical, the branch soon bends back; if the disturbances in an experiment were large enough, the planar interface might jump to some finite-amplitude state before the pulling speed reaches $\mathcal{V}_c$, suggesting that the bifurcation were subcritical even though Wollkind and Segel[6] (correctly) predict that it is supercritical. As $\Delta\mathcal{C}$ moves through the transition point, the bifurcation structure at $\mathcal{V}=\mathcal{V}_c$ changes from supercritical to subcritical as is shown in the final frame of Fig. 9(a).

Figure 9(b) shows the bifurcation structure of region IV. Here $\Delta n<0$, and the transition point lies on the upper branch of the neutral stability curve. The first frame shows a disconnected set of solutions existing for a negative value of $\Delta\mathcal{C}$. At the limit point, $\Delta\mathcal{C}=0$, this solution moves in and meets the axis at a point $\mathcal{V}=\mathcal{V}_c=\mathcal{V}_a$. For a positive value of $\Delta\mathcal{C}$, but below the transition point, $\mathcal{V}_c$ and $\mathcal{V}_a$ split to form two subcritical solution branches similar to Fig. 9. For a value of $\Delta\mathcal{C}$ above the transition point the bifurcation structure at $\mathcal{V}=\mathcal{V}_a$ changes its type from subcritical to supercritical.

A different type of bifurcation structure exists in region V, and is shown in Fig. 10(a). Here $\Delta n>0$, so the transition point is located on the lower branch of the neutral stability curve and the second Landau coefficient a_2 is positive. The bifurcation structure now depends on another parameter p,

$$p=\frac{\beta_2}{2(\alpha_2 a_2)^{1/2}}-1\ . \tag{5.1}$$

In this region $p>0$ (see Table I). When operating to the left of the limit point, i.e., at a negative value of $\Delta\mathcal{C}$, a subcritical isola moves in from infinity. Unlike the previous cases the analysis now describes the stable solution to which large enough disturbances jump. As $\Delta\mathcal{C}$ is increased, this disconnected solution moves towards the axis. At $\Delta\mathcal{C}=0$ the planar interface becomes unstable at a point $\mathcal{V}=\mathcal{V}_c=\mathcal{V}_a$. For positive values of $\Delta\mathcal{C}$, but below the transition point, the connected supercritical state grows larger until, simultaneously, both solution branches meet and there is a change of the type of the bifurcating solution at $\mathcal{V}=\mathcal{V}_c$, from supercritical to subcritical as $\Delta\mathcal{C}$ crosses the transition point.

In region VI, $\Delta n>0$, and the transition point is located on the upper branch of the neutral stability curve. This is the subcritical case of the previous example. In Fig. 10(b), for a negative value of $\Delta\mathcal{C}$ a disconnected subcritical isola exists. The next frame shows how, at $\Delta\mathcal{C}=0$, this isola moves into the axis showing locally, at $\mathcal{V}=\mathcal{V}_c=\mathcal{V}_a$, two transcritical solutions. For positive values of $\Delta\mathcal{C}$ the critical pulling speeds split and two subcritical solution branches are formed. Once $\Delta\mathcal{C}$ is beyond the transition point, the bifurcation structure at $\mathcal{V}=\mathcal{V}_a$ changes to supercritical.

Region VII is characterized by a positive Δn and a negative value of p, and the bifurcation structure present is shown in Fig. 11(a). There is no subcritical disconnected solution. When $\Delta\mathcal{C}=0$ the planar interface becomes unstable only at the point $\mathcal{V}=\mathcal{V}_c=\mathcal{V}_a$, which splits on increasing $\Delta\mathcal{C}$ to form supercritical bifurcation at each branch. When $\Delta\mathcal{C}$ is increased beyond the transition point the bifurcating solution at $\mathcal{V}=\mathcal{V}_c$ changes to subcritical but the analysis still describes the full loop.

In the final region, region VIII, the bifurcation structure is as shown in Fig. 11(b). For a very negative value of $\Delta\mathcal{C}$ there are no disconnected solution sets. As $\Delta\mathcal{C}$ is increased, but still below the limit point, an isola grows from a point when

$$\Delta\mathcal{C}=\frac{\alpha_2\beta_1^2(\Delta n)^2}{\alpha_1\beta_2^2}\left[1-\frac{4\alpha_2 a_2}{4\alpha_2 a_2-\beta_2^2}\right], \tag{5.2}$$

and increases in size with increasing $\Delta\mathcal{C}$. Thus, even though linear theory predicts stability there exists a

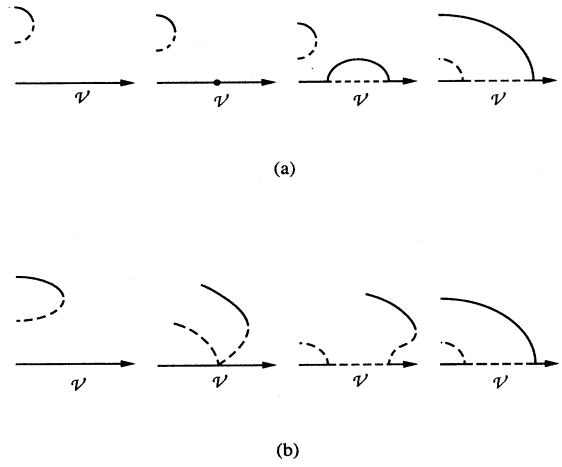

FIG. 10. Bifurcation diagram corresponding to amplitude equation (4.25). The dashed lines represent unstable solutions. (a) region V of Fig. 7; (b) region VI of Fig. 7.

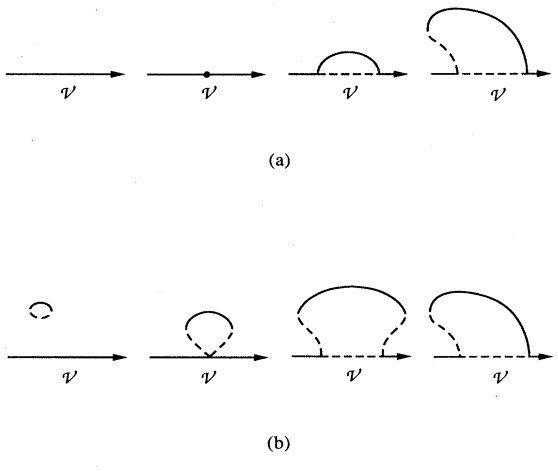

FIG. 11. Bifurcation diagram corresponding to amplitude equation (4.25). The dashed lines represent unstable solutions. (a) region VII of Fig. 7; (b) region VIII of Fig. 7.

finite-amplitude steady state. By further increasing $\Delta\mathcal{C}$ the isola moves into the axis until $\Delta\mathcal{C}=0$, where it meets the axis forming two locally transcritical solution branches. For positive values of $\Delta\mathcal{C}$ the critical pulling speeds split to form a subcritical "mushroom." When $\Delta\mathcal{C}$ moves above the transition point, the bifurcating solution at $\mathcal{V}=\mathcal{V}_a$ changes type to supercritical. This is shown in the final frame of Fig. 11(b).

VI. DISCUSSION

By introducing length and time scales independent of V and c_∞, we are able to obtain linear-stability curves for directional solidification that resemble the dimensional ones as shown for fixed G in Fig. 2. Here the limit point of the curve has coordinates $(\mathcal{C}^*,\mathcal{V}^*)$. The transition point separates supercritical from subcritical bifurcation behavior.

We examine the system with negligible latent heat and describe two-dimensional bifurcations from the planar interface when $\mathcal{C}$ is near $\mathcal{C}^*$. We choose $\mathcal{C}$ near $\mathcal{C}^*$, since we are then able to describe the bifurcations from the two branches simultaneously. Two cases are examined.

(i) When the transition point is distant from the limit point, we find the amplitude equation (4.23), which has cubic nonlinearities and a Landau constant a_1. If the transition point is on the lower branch, then $a_1>0$ and the bifurcations from both branches are supercritical as shown in Fig. 8(a). If the transition point is on the upper branch, as it is for larger conductivity ratios n, $n=k_S/k_L$, then both bifurcations are subcritical as shown in Fig. 8(b). Both of these are discussed in Sec. V.

(ii) When the transition point is coalescent with the limit point, then $a_1=O(\epsilon^2)$ and we find the generalized amplitude equation (4.25), which has both cubic and quintic nonlinearities and a second Landau coefficient a_2. Both a_1 and a_2 depend on n and k only since latent heat is neglected. Figure 7 shows the parametric regions in which the Landau constants take on various possible signs and Figs. 8–11 give the bifurcation patterns that emerge. These are discussed in Sec. V.

The light curve in Fig. 7 indicates, in parameter space, where the transition point is coalescent with the limit point, this occurs only when the conductivity ratio is relatively large. For example if $k=0.5$, then n must be about 3; for other values of k, n must be larger yet. We have considered the coalescent case for two reasons. First, as is clear, it allows for a much richer variety of behaviors to occur. Second, despite the technical necessity of bringing the transition point into the asymptotic region of the analysis, the resulting behavior should be suggestive of the bifurcation structure near the transition point even if it is not close to the limit point. For example the band width around the zero of a_1 in Fig. 7 is proportional to $\Delta\mathcal{C}$, and if $\Delta\mathcal{C}$ is no longer small, regions III through VIII may correspond to physically meaningful parameter ranges.

The results of the present analysis should be useful in rationalizing existing bifurcation theories and the results of numerical simulations. Rapid turn arounds, as seen for example in Fig. 9(a), may be hard to resolve numerically since these schemes often have some form of gridscale error.[20] Our results can be used as qualitative test cases for various types of simulations.

Our Figs. 8 and 11 have superficial resemblances to those of Haug.[13] However, the physical situations and consequences are quite different. Haug considered two-dimensional bifurcation in a channel of width W (in the x direction) where sidewalls allow only *a few* cell wavelengths. Thus, W is of the order D/V. He then selects special values of W, W_0 say, that allow two modes to become unstable simultaneously (codimension 2 bifurcation) or only one mode unstable (codimension 1 bifurcation). All the normal forms present is his model are then classified by using imperfect bifurcation theory. His analysis does not focus on the limit point of the neutral stability curve. The present analysis considers the infinite range on x since there are no sidewalls, and in a neighborhood of $\mathcal{C}^*$ examines simultaneously the bifurcations from the lower and upper branches of the neutral stability curve.

ACKNOWLEDGMENTS

The authors would like to thank D. S. Riley and P. W. Voorhees for some helpful discussions. This work was supported by a grant from the National Aeronautics and Space Administration Program on Microgravity Science and Applications.

APPENDIX A

In the notation of Alexander *et al.*[7] the corrected form of the Landau coefficient a_1 is

$$\begin{aligned}\mathrm{Re}(a_1)=&\left[\frac{k(k-1)}{16}-k(k-1)(\zeta_{11}+\tfrac{1}{2}\zeta_{20})-kA_{11}\right.\\&+A_{10}(2\omega^2\zeta_{20}-\tfrac{1}{4}\omega^2M_{10})+\omega^2A_{20}-\frac{M_{20}A_{20}}{2}(M_{20}+k-1)\\&\left.+(M_{10}+k-1)\left[A_{11}-(1-k)\zeta_{11}+\frac{M_{20}A_{20}}{2}-\frac{(1-k)}{2}\zeta_{20}-\frac{(k-1)}{16}-\frac{3\omega^4(k-1)A}{16k}-\frac{4\zeta_{20}\omega B_{10}}{n+1}\right]\right]\\&\times\left[\frac{k-1}{2}+\frac{A_{10}}{2M_{10}-1}+\frac{(k-1)(M_{10}+k-1)}{2I\omega}\right]^{-1},\end{aligned}\tag{A1}$$

where

$$A_{10}=\frac{-k(k-1)}{2(M_{10}+k-1)}\ , \tag{A2}$$

$$M_{10}=\tfrac{1}{2}+(\tfrac{1}{4}+\omega^2)^{1/2}\ , \tag{A3}$$

$$M_{20}=\tfrac{1}{2}+(\tfrac{1}{4}+4\omega^2)^{1/2}\ , \tag{A4}$$

$$B_{10}=\frac{(k-1)(n+1)}{4I}-\frac{(n-1)(k-1)G}{4}\ , \tag{A5}$$

$$A_{20}=\frac{k-1}{2}+\frac{M_{10}A_{10}}{2}-(k-1)\zeta_{20}\left[1-G-4\omega^2\frac{A}{k}\right]\ , \tag{A6}$$

$$\zeta_{20}=\left[[2\omega^2+M_{10}(1-M_{20})]\frac{A_{10}}{2}+\tfrac{1}{8}(k-1)(1-M_{20})\right]\times\left\{(k-1)\left[k-(M_{20}+k-1)\times\left[1-G-4\omega^2\frac{A}{k}\right]\right]\right\}^{-1}\ , \tag{A7}$$

$$A_{11}=-(k-1)\zeta_{22}-\frac{k(k-1)M_{10}}{4(M_{10}+k-1)}+\frac{k-1}{8}\ , \tag{A8}$$

$$\zeta_{11}=\frac{\omega(1-n)}{4(n+1)}+\frac{\omega I^{-1}}{2(G-I^{-1})(n+1)}\ . \tag{A9}$$

APPENDIX B

The coefficients appearing in the approximate dispersion relation (2.10) are

$$\alpha_1=\frac{2a^{*2}H(2a^{*2}-k\mathcal{V}^{*2})}{2a^{*2}H+k\mathcal{V}^{*2}}\ , \tag{B1}$$

$$\alpha_2=\frac{(H+\lambda_1)(2a^{*2}H^2-k\lambda_1\mathcal{V}^{*3})}{H^2(2a^{*2}H+k\mathcal{V}^{*3})}\ , \tag{B2}$$

$$\alpha_3=-a^*[4\mathcal{V}^*-2\mathcal{C}^*\mathcal{V}^{*2}(1+n)+2a^{*2}\mathcal{V}^*(1+n)+H^2(1+n)(2\mathcal{C}^*-\mathcal{V}^*)+H^3(1-2k)(1+n)]\times\{H^2[2+(1+n)(a^{*2}-\mathcal{C}^*\mathcal{V}^*+\mathcal{C}^*H]\}^{-1}\ , \tag{B3}$$

$$\alpha_4=\{nH^4-8a^{*4}(1+n)-16a^{*2}+2H^2[2+5(1+n)a^{*2}-(1+n)\mathcal{C}^*\mathcal{V}^*]+H^3[2(\lambda_1-\mathcal{V}^*)+2k\mathcal{V}^*(1+n)-n\mathcal{V}^*]+8a^{*2}\mathcal{C}^*\mathcal{V}^*(1+n)\}\times\{2H^2[2+(1+n)(a^{*2}-\mathcal{C}^*\mathcal{V}^*-\mathcal{C}^*H)]\}^{-1}\ , \tag{B4}$$

where

$$H=\mathcal{V}^*-2\lambda_1\ , \tag{B5}$$

$$\lambda_1=\tfrac{1}{2}[\mathcal{V}^*+(\mathcal{V}^{*2}+4a^{*2})^{1/2}]\ , \tag{B6}$$

and $\mathcal{C}^*$, $\mathcal{V}^*$, and a^* are given in Eq. (2.6).

APPENDIX C

The functions $F_1(k)$ and $F_2(k)$ appearing in the Landau coefficient a_1 in Eq. (4.14) are

$$F_1=[-4h_{22}+\hat{C}k\hat{V}^4+\hat{C}k\hat{\lambda}_1\hat{V}^3(k\hat{V}^2-2)]\left[\frac{2(2\hat{\lambda}_1-\hat{V})}{\hat{C}\hat{V}[2(2\hat{\lambda}_1-\hat{V})-k\hat{V}^3]}\right]\ , \tag{C1}$$

$$F_2=(-4\hat{C}c_{22}[\hat{\lambda}_2(k\hat{V}^2-2)+2\hat{V}]-2\hat{C}\hat{V}h_{22}[3k\hat{V}^2-k\lambda_1\hat{V}(k\hat{V}^2-2)-4]+\{\hat{C}k\hat{\lambda}_1\hat{V}^4(k\hat{V}^2-3)-[12+\hat{C}\hat{V}^3(2+3k)(k\hat{V}^2-2)]\})\left[\frac{(2\hat{\lambda}_1-\hat{V})}{2\hat{C}\hat{V}[2(2\hat{\lambda}_1-\hat{V})-k\hat{V}^3]}\right]\ , \tag{C2}$$

where

$$q=\tfrac{1}{2}[4k-1+(1+8k)^{1/2}]\ , \tag{C3}$$

$$\hat{V}=\frac{2}{q^{1/2}}\ , \tag{C4}$$

$$\hat{C}=\frac{q^{3/2}}{q-2k}\ , \tag{C5}$$

$$\hat{\lambda}_1=\tfrac{1}{2}[\hat{V}+(\hat{V}^2+4)^{1/2}]\ , \tag{C6}$$

$$\hat{\lambda}_2=\tfrac{1}{2}[\hat{V}+(\hat{V}^2+16)^{1/2}]\ , \tag{C7}$$

$$T_1=(6-\hat{C}k\hat{V}^3)[\hat{\lambda}_1-\hat{V}(1-k)]+2\hat{C}k\hat{V}^2\ , \tag{C8}$$

$$h_{22}=\frac{\hat{C}\hat{V}^2}{T_1}\{-k\hat{V}(1+\hat{\lambda}_1\hat{V}k)-[\hat{\lambda}_2-\hat{V}(1-k)](1-k\hat{\lambda}_1\hat{V})\}\ , \tag{C9}$$

$$c_{22}=-k\hat{V}^3(T_1(1+k\hat{\lambda}_1\hat{V})-2\hat{C}\hat{V}\{(1-k\hat{\lambda}_1\hat{V})[\hat{\lambda}_2-\hat{V}(1-k)]+\hat{V}k(1+k\hat{\lambda}_1\hat{V})\})\{2T_1[\hat{\lambda}_2-\hat{V}(1-k)]\}^{-1}\ . \tag{C10}$$

[1]W. J. Boettinger, D. Shechtman, R. J. Schaefer, and F. S. Biancaniello, Metall. Trans. A **15**, 55 (1984).

[2]R. Trivedi, J. A. Sekhar, and V. Seetharaman, Metall. Trans. A **20**, 769 (1989).

[3]W. W. Mullins and R. F. Sekerka, J. Appl. Phys. **35**, 444 (1964).

[4]S. R. Coriell and R. F. Sekerka, in *Rapid Solidification Processing Principles and Technologies II,* edited by R. Mehrabian, B. H. Kear, and M. Cohen (Claitor's Publishing Division, Baton Rouge, LA, 1980).

[5]S. R. Coriell, G. B. McFadden, and R. F. Sekerka, Annu. Rev. Mater. Sci. **15**, 119 (1985).

[6]D. J. Wollkind and L. A. Segel, Philos. Trans. R. Soc. London **268**, 351 (1970).

[7]J. I. D. Alexander, D. J. Wollkind, and R. F. Sekerka, J. Cryst. Growth **79**, 849 (1986). There are a few typographical errors in the Landau coefficient a_1; a corrected version is given in Appendix A.

[8]G. J. Merchant and S. H. Davis, Phys. Rev. Lett. **63**, 573 (1989).

[9]G. I. Sivashinsky, Physica **D8**, 243 (1983).

[10]K. Brattkus and S. H. Davis, Phys. Rev. B **38**, 11 452 (1988).

[11]D. S. Riley and S. H. Davis, SIAM (Soc. Ind. Appl. Math) J. Appl. Math. (to be published).

[12]L. H. Ungar and R. A. Brown, Phys. Rev. B **29**, 1367 (1984).

[13]P. Haug, Phys. Rev. A **35**, 4364 (1987).

[14]M. J. Bennett and R. A. Brown, Phys. Rev. B **39**, 11 705 (1989).

[15]F. X. Kelly and L. H. Ungar, Phys. Rev. B **34**, 1746 (1986).

[16]R. A. Brown, AIChE J. **34**, 881 (1988).

[17]B. Caroli, C. Caroli, and B. Roulet, J. Phys. (Paris) **43**, 1767 (1982).

[18]D. Dellwo, H. B. Keller, B. J. Matkowsky, and E. L. Reiss, SIAM (Soc. Ind. Appl. Math) J. Appl. Math. **42**, 956 (1982).

[19]M. Golubitsky and W. F. Langford, J. Differ. Equ. **41**, 375 (1981).

[20]A. A. Wheeler and K. H. Winters (unpublished).